Macromolecules

ARTICLE

pubs.acs.org/Macromolecules

Development of Intermolecular Structure and Beta-phase of Random Poly[9,9-bis(2-ethylhexyl)fluorene]-*co*-(9,9-dioctylfluorene) in Methylcyclohexane

Matti Knaapila,[†,*] Daniel W. Bright,[‡] Benjamin S. Nehls,[§] Vasil M. Garamus,[⊥] László Almásy,[∥] Ralf Schweins,[#] Ullrich Scherf,[▽] and Andrew P. Monkman[‡]

[†]Physics Department, Institute for Energy Technology, NO-2027 Kjeller, Norway

[‡]Department of Physics, University of Durham, DH1 3LE Durham, England

[§]BASF-SE, DE-67056 Ludwigshafen, Germany

[⊥]Helmholtz-Zentrum Geesthacht, Zentrum für Material- und Küstenforschung GmbH, DE-21502 Geesthacht, Germany

[∥]Research Institute for Solid State Physics and Optics, Budapest-1525, Hungary

[#]Institut Laue-Langevin, DS/LSS Group, 38042 Grenoble Cedex 9, France

[▽]Fachbereich Chemie, Bergische Universität Wuppertal, DE-42097 Wuppertal, Germany

ABSTRACT: We present small-angle neutron scattering (SANS) and optical absorption studies of random poly[9,9-bis(2-ethylhexyl)fluorene]-*co*-(9,9-dioctylfluorene) (PF2/6-F8) mixed with deuterated methylcyclohexane (MCH-d_{14}) at room temperature. The polymers studied have identical main chains and the same number of side chain carbons, but they differ in terms of side chain branching such that the fraction of F8 repeat units with linear octyl side chains was 50, 90 or 95%. Poly[9,9-bis(2-ethylhexyl)fluorene] (PF2/6) and poly(9,9-dioctylfluorene) (PF8) homopolymers were studied for comparison. On the scale of 100 nm or less, the data imply that PF2/6 and PF2/6-F8 (50:50) appear as separated stiff chains (the diameter of the order of 1 nm). PF8 and PF2/6-F8 (10:90 and 5:95) aggregate into stiff sheetlike aggregates (the lateral size of tens of nanometers, the thickness of about 2 nm). This aggregation tendency is an inverse function of side chain branching. On scales over 100 nm, the locally dissolved polymers overlap and form macroscopically isotropic network. In contrast, the polymer sheets form cross-linked ribbonlike agglomerates. This tendency, too, varies with the degree of side chain branching. The extent of β-phase follows the existence of sheetlike structures increasing sharply with increasing F8 content.

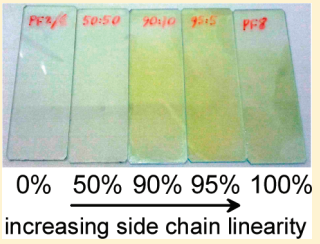

1. INTRODUCTION

Polyfluorene homopolymers[1] have long represented a central class of π-conjugated polymers due to their stability and optoelectronic performance. However, rather than using homopolymers in applications, the electronic structure of polyfluorenes is frequently tailored by copolymerization (see an illustrative example in ref 2) where fluorene units are incorporated in π-conjugated copolymers; polymers that are used for example in organic photovoltaic cells,[3] field-effect transistors,[4] light emitting diodes[5] and white organic light emitting device applications,[6] to mention a few. As these devices are processed from solutions, structural and phase behavioral studies concern both the solid state and solutions[7] and gels alike[8] but still the most detailed efforts are placed on archetypical homopolymers such as branched side chain poly[9,9-bis(2-ethylhexyl)fluorene] (PF2/6)[9,10] or linear side chain poly(9,9-dioctylfluorene) (PF8)[11,12] (Figure 1). The effects of the molecular weight[13] and side chain length[14] on the structure and phase behavior of homopolyfluorenes have been established. This is not surprising as homopolymers have provided an easier route for understanding of underlying physics. The importance of understanding copolymers incorporating PF8 is, however, manifold, given the extensive use of this motif as a solubilizing group in complex white emitters[6] and how the different structures of these polymers control electro-optical properties such as exciton mobility.[15] Also important are the application of structural engineering to localize excitons within low energy ordered β phase regions to enhance lasing[16] and the tailoring of both optical and electrical properties simultaneously using copolymers having different side chain structures[17] or iridium complexes.[18] Copolymerization is also a tool for cross-linking PF8.[19] Also known are copolymers containing PF2/6 and anthracene,[20] for example.

Cheun et al.[21] studied random poly[9,9-bis(2-ethylhexyl)-fluorene]-*co*-(9,9-dioctylfluorene) (PF2/6-F8) (Figure 1) and showed how their optical properties lie between those of the PF2/6 and PF8 homopolymers which have completely different solid state structures. Distinctly, PF2/6 always adopts a characteristic helical backbone[22] whereas PF8 is linear and can adopt nearly planar backbone leading to a significant new low energy optical absorption and emission band classified as β phase.[11,23]

Received: June 2, 2011
Revised: July 13, 2011
Published: August 01, 2011

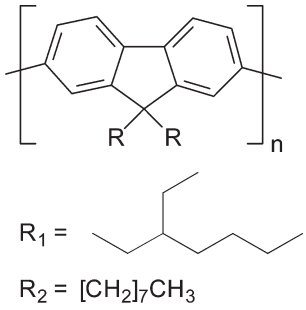

Figure 1. Chemical structures of PF2/6 with branched ethylhexyl side chains (R_1) and PF8 with linear octyl side chain (R_2). The PF2/6-F8 copolymers contain randomly distributed F2/6 monomers [with R_1] and F8 monomers [with R_2]. In the present study, these monomers were mixed with the molar ratios (F2/6:F8) of 50:50, 10:90, and 5:95.

Cheun et al. showed in particular how increasing the content of F8 monomers significantly increases the extent of β phase, suppresses the extent of conformational disorder (and the effective electron−phonon coupling strengths) and presumably alters the structure in the solid state bulk.

Bright et al.[24] studied random poly(9,9-dioctylfluorene)-*co*-dibenzothiophene (PF8-DBT), including DBT both with and without *S,S*-dioxide in the monomer, in toluene vapor exposed films. The authors showed that the amount of β phase decreases with increasing DBT content to a cutoff of 12% and 20% with and without *S,S*-dioxide, respectively. The polymers with increasing DBT content show a smooth linear drop in the β phase characteristics.

Elsewhere, we studied structural differences between PF2/6 and PF8 in 1 vol % methylcyclohexane (MCH) after a heating-cooling cycle.[25] The heating ensures the formation of isotropic mixture and resets the thermal history, while the cooling accelerates β phase formation as illustrated for the dilute solutions by Dias et al.[26] By using small-angle neutron scattering (SANS) we found how PF2/6 appears as separated free chains whereas PF8 assembles into sheetlike aggregates with high β phase fraction with the assumed lateral size of tens of nanometers. When studying PF8 in MCH, Chen et al.[27] found out moreover that PF8 sheets appear in a lyotropic phase with interconnected morphology coexisting with the solvent phase. After further refinement with SANS and X-ray diffraction[28] we confirmed this result and proposed that PF2/6 remains as a network of overlapping but locally not ordered chains whereas the PF8 sheets are joined together forming ribbonlike agglomerates cross-linking to a fractal network structure.

While PF8 and PF2/6 represent the extreme cases in MCH, the question of the intermediate stages is naturally raised. In one study, we used PF2/6-F8 random copolymers and showed that adding 50% of F8 units maintains the isotropic phase of locally free chains while 90% addition reverts polymer to the sheetlike aggregates.[14] Random copolymers provide a definitively non phase segregated system with varying degree of side chain branching. Two aspects remain open. First, it is not known how the PF2/6-F8 copolymer system or PF2/6 behaves at length scales larger than individual sheets. Second, there is no information on the evolution of the β phase fraction of PF8 in MCH, while this is important to understand how random copolymers will behave.

In this brief paper, we employ SANS and optical spectroscopy to study how PF2/6-F8 random copolymers behave in deuterated MCH (MCH-d_{14}) at room temperature. The q-range 0.00058−0.25 Å^{-1} was selected to cover both the length scales of individual sheets and polymers as well as their larger agglomerates. The fraction of F8 units and thus side chain linearity was set at 50%, 90%, or 95%. PF2/6 and PF8 homopolymers were studied for comparison. PF2/6 forms an isotropic mixture of locally free chains while PF8 forms a fractal network of polymer sheets. We propose that copolymers form structures between these extremes, the network showing increasing openness with higher side chain branching. A transition from the isotropic mixture to the agglomerates of sheetlike aggregates takes place between 50% and 90% addition of F8 units. The extent of β phase follows the existence of sheetlike structures, systematically increasing with increasing F8 content. These results complement findings of previous reports and provide an insight into how a gradual increase of side chain linearity has surprisingly large influence on the solution structure.

Table 1. Molecular Characteristics of Studied Samples[a]

material	M_n (kg/mol)	M_w (kg/mol)	c (vol %)	c^* (vol %)
PF2/6	43	83	1.0	0.21 ± 0.02
PF2/6-F8 (50:50)	>5	-	1.0	-
PF2/6-F8 (10:90)	>5	-	1.0	-
PF2/6-F8 (5:95)	>5	-	1.0	-
PF8	47	153	1.0	0.16 ± 0.01

[a] M_n and M_w are number and weight averaged molecular weight. c and c^* are the polymer concentration and polymer overlapping concentration, respectively.

2. EXPERIMENTAL SECTION

2.1. Sample Preparation. The chemical structures of used polymers are shown in Figure 1. PF2/6 and PF8 were prepared following the Yamamoto-type polycondensation of the corresponding 2,7-dibromo-9,9-dialkylfluorenes with Ni(COD)$_2$ as outlined in ref 1. The PF2/6-F8 random copolymers were prepared as described in ref 21. The applied molar ratios of F2/6 and F8 repeat units were 50:50, 10:90, and 5:95. The corresponding polymers are denoted as PF2/6$_{0.50}$-F8$_{0.50}$, PF2/6$_{0.10}$-F8$_{0.90}$ and PF2/6$_{0.05}$-F8$_{0.95}$. The molecular characteristics of these polymers are compiled in Table 1. The molecular weights were determined using gel permeation chromatography.

Following the argumentation of Ying and Chu[29] the polymer overlapping concentration is defined as a number of molecules per unit of volume as

$$c^* = M_n/(N_A(2R_g)^3) \quad (1)$$

where R_g is the radius of gyration of a single polymer in dilute solution. M_n is the number-averaged molecular weight of the polymer and M_n/N_A represents a weight of a single molecule.

The radius of gyration can be estimated from the Kratky−Porod equation for worm-like polymers as

$$R_g^2 \sim l_0 l_p M_n/3M_0 \quad (2)$$

where l_0 and l_p are the length of repeat unit and the persistence length. M_0 is the weight of the repeat unit.

The polymer overlap concentrations for the limiting cases (PF8 and PF2/6) were calculated using eqs 1 and 2. The used repeat and persistence lengths were 8.1 Å[22] and 70 Å[9] for PF2/6 and 8.3 Å[30] and 98 Å[31] for PF8, respectively. The total lengths of the polymers are of the order of 1000 Å, as estimated from the repeat lengths and molecular weights.

For neutron scattering, the polymers were dissolved in MCH-d_{14} (99.5% D, Apollo Scientific Ltd.). The employed concentration c was 10 mg/mL corresponding to a 1.0 vol % or 1.3 wt % mixture. The mixtures were prepared via a heating−cooling cycle, which ensures nominally isotropic solution at the elevated temperature and subsequent gelation[25] at low temperature. In a typical procedure, the mixtures were first heated up to 80−85 °C and stirred at 1000 rpm for 1 h until completely clear solutions were observed. These samples were cooled from 80 to 85 °C down to −25 °C for 1 h and subsequently warmed to 20 °C in about 10 min before measurements which were carried out immediately afterwards. In this procedure, PF2/6/MCH-d_{14} and PF2/$6_{0.50}$-$F8_{0.50}$ appear as transparent yellowish liquids at 20 °C, while the other mixtures become turbid and gel-like.

2.2. SANS Measurements. A part of SANS measurements was performed at the instrument D11 at the Institut Laue-Langevin (ILL) in Grenoble, France. A wavelength of 6 Å with sample-to-detector distances of 8 and 34 m and a wavelength of 16.5 Å with a sample-to-detector distance of 34 m were used. These settings provided a q-range of 0.00058−0.02 Å^{-1}. Another part of SANS measurements was performed using the SANS-1 instrument at the Helmholtz-Zentrum Geesthacht in Geesthacht, Germany,[32] and merged with the ILL data. Several sample-to-detector distances (from 0.7 to 9.7 m) and wavelength 8.1 Å were employed to cover a q-range of 0.004−0.25 Å^{-1}. The raw scattering patterns were corrected by conventional procedures.[33] The incoherent scattering from polymer hydrogen was taken into account by using a 1:99 mixture of MCH: MCH-d_{14} as a background.

The initial consideration of SANS data was made using scaling arguments. The scattering intensity I follows the relation

$$I(q) \sim q^{-\alpha} \tag{3}$$

where the scattering exponent $\alpha = 1$ indicates the presence of separated rodlike particles and $\alpha = 2$ of sheetlike particles.

For more complex structures, the scattering exponent is related to the dimensions of mass and surface fractals as $\alpha = 2D_m - D_s$.[34] The exponent $1 < \alpha < 3$ refers to the mass fractal system with the fractal dimension $D_m = \alpha$. The exponent $3 < \alpha < 4$ refers to the surface fractal with the dimension $D_s = 6 - \alpha$.

When α approached unity thus pointing to rodlike particles at higher q-range, the data were fitted to a model of rodlike particles using the software GNOM.[35]

A two-component model fitted to the entire scattering curve was employed to describe the whole system. The low q part of the curve was fitted to the Debye−Bueche equation[36]

$$I(q) \sim \frac{1}{(1 + \xi_s^2 q^2)^2} \tag{4}$$

where ξ_s is a characteristic length scale in a continuous two-phase system. When the sample was expected to contain rodlike particles, the high q part was fitted to the equation[12]

$$I(q) \sim \frac{1}{1 + \xi_d q \exp(q^2 R^2/4)} \tag{5}$$

where ξ_d represents the mesh size of the dynamic network and R the radius of the rodlike particle, ultimately the radius of a single rodlike polymer. When the sample was expected to contain sheetlike particles, the high q part was fitted to the equation[14]

$$I(q) \sim \frac{1}{1 + \xi_{sheet}{}^2 q^2 \exp(q^2 L^2/12)} \tag{6}$$

where ξ_{sheet} and L are the size and thickness of polymer sheets.

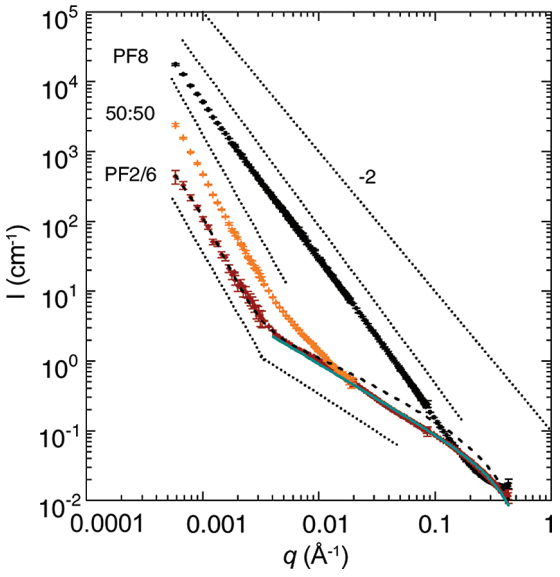

Figure 2. SANS patterns of PF2/6 (brown diamonds), PF8 (black squares) and F8−F2/6 copolymer with the F2/6:F8 ratio 50:50 (orange up triangles) mixed with MCH-d_{14} (c = 10 mg/mL). Cyan solid line and black dashed lines, respectively, are the fits to the IFT model and to the two-component model of PF2/6 data with the assumption of rodlike polymers (see Experimental Section for details). Black dotted lines show the best linear fits (offset for clarity) and −2 slope for comparison.

The interconnected polymer chains can also be considered as a random network similar to fractal structures. The scattering intensity can be written as[37]

$$I(q) \sim 1 + \frac{1}{(qr_0)^{\alpha}} \frac{\alpha\Gamma(\alpha - 1)}{(1 + 1/(q^2 \xi_{agglomerate}{}^2))^{(\alpha - 1)/2}} \sin[(\alpha - 1)\tan^{-1}(q\xi_{agglomerate})] \tag{7}$$

where r_0 is the characteristic size of the primary scatterers, $\xi_{agglomerate}$ represents the overall size of the fractal objects (denoted here as agglomerates), α is the fractal dimension, and $\Gamma(x)$ is the gamma function.

2.3. Optical Absorption Measurements. Optical absorption spectra of the polymers in 10 mg/mL MCH solution were measured using a Shimadzu UV-3600 spectrophotometer over 320−500 nm at 0.5 nm intervals. The sample cells comprised two new precleaned microscope slides. For each polymer, hot isotropic solution (∼90 °C) was added onto one slide while the second was pressed on top and the edges were clamped together. The samples were left at room temperature for 10 min and initial absorption spectra were measured. The samples were subsequently placed in a dewar filled with dry ice for 45 min. The outer surfaces of the slides were then deiced using compressed air and equilibrated back to room temperature. The absorption spectra were measured at room temperature. The absorption spectrum of the blank slides was subtracted as a background. Data were fitted to the spectral peaks corresponding to free polymer and polymer assemblies with and without β phase, as outlined in ref 28.

3. RESULTS AND DISCUSSION

Figure 2 shows the SANS patterns of 10 mg/mL PF2/6/MCH-d_{14}, PF8/MCH-d_{14}, and F2/$6_{0.50}$- $F8_{0.50}$/MCH-d_{14} with the q-range of 0.00058−0.25 Å^{-1}. Best linear fits illustrate the apparent straight sections of data. Also shown are the IFT fits and

Table 2. Parameters Estimated from the Fits to the SANS Data of PFs in MCH-d_{14} (c = 10 mg/mL)[a]

	analyzed q-range (Å^{-1})	PF2/6	PF2/6-F8 (50:50)		PF2/6-F8 (10:90)	PF2/6-F8 (5:95)	PF8
α	0.00058−0.004	2.67 ± 0.04	2.97 ± 0.02		2.88 ± 0.06	3.63 ± 0.07	2.27 ± 0.01
	0.00058−0.1						2.26 ± 0.01
	0.004−0.02	1.01 ± 0.01	1.81 ± 0.02		2.13 ± 0.02	1.94 ± 0.01	2.23 ± 0.01
	0.004−0.04	1.07 ± 0.01					
model		rod	rod	sheet	sheet	sheet	sheet
ξ_s (Å)	0.00058−0.1	1751 ± 14	1981 ± 36	2065 ± 21	2848 ± 56	2368 ± 23	
ξ_d (Å)		287 ± 162	544 ± 42				
R (Å)		∼5	∼5				
ξ_{sheet} (Å)				359 ± 21	476 ± 14	194 ± 13	
L (Å)				∼5	∼10	∼10	
$R_{CS,g}$ (Å)	0.004−0.43	∼3					
D_{max} (Å)		∼10					
α	0.00058−0.004				2.76 ± 0.02	3.09 ± 0.02	
$\xi_{agglomerate}$					>6000	>1985	
r_0					361 ± 24	278 ± 9	

[a] Linear fit: α is the exponent for given q-range. A multi-component model: ξ_s is connected to the larger length scale density fluctuations. ξ_d and R are the mesh size and the and the radius of a rodlike polymer while ξ_{sheet} and L represent the lateral size and thickness of polymer sheet. GNOM: $R_{CS,g}$ and D_{max} represent the cross-sectional radius of gyration and the maximal cross-sectional size of a rodlike scatterer. General fractal objects: α is the fractal dimension while the parameters $\xi_{agglomerate}$ and r_0 represent the overall size of fractal agglomerates and the size of primary aggregates.

the fits to the two-component model (eqs 4-5) for the rodlike polymers for the data of PF2/6/MCH-d_{14}. Table 2 shows the parameters estimated from these fits.

The data of PF8/MCH-d_{14} correspond to those shown in ref 28. The data of PF2/6/MCH-d_{14} and F2/6$_{0.50}$-F8$_{0.50}$/MCH-d_{14} correspond to those shown in refs 14 and 25, but the studied q-range is significantly wider than that in earlier reports (>0.004 Å^{-1}). This allows an identification of not only polymer chains and polymer aggregates but also the agglomerations of these aggregates. In this classification, polymer chains and aggregates are understood to be relatively compact entities behaving as single scatterers while the polymer agglomerates are understood as loose networks of polymer aggregates.

We consider first the q-range for >0.004 Å^{-1}. The SANS patterns shown in Figure 2 are completely dissimilar. The data of PF8/MCH-d_{14} scale predominantly as q^{-2} over the whole q-range, whereas the data of PF2/6/MCH-d_{14} scales as q^{-1} for q > 0.004 Å^{-1} showing a distinctive upturn for smaller scattering angles. Also, the scattering intensity is significantly higher for PF8 compared to PF2/6 for q < 0.1 Å^{-1} only approaching each other for q > 0.1 Å^{-1}. These observations are in agreement with our earlier observations[25] and point to the existence of sheetlike PF8 assemblies and separated rodlike PF2/6 polymers. The scattering curve of PF2/6$_{0.50}$-F8$_{0.50}$MCH-d_{14} follows a path in between the data of PF8/MCH-d_{14} and PF2/6/MCH-d_{14}, but the overall behavior resembling more that of PF2/6/MCH-d_{14}. Thus, PF2/6$_{0.50}$-F8$_{0.50}$/MCH-d_{14} appears locally as separated free chains.

We consider next the q-range <0.004 Å^{-1}. The scattering curve of PF8/MCH-d_{14} follows −2 decay and this has been interpreted as an indication of a fractal network of polymer sheets.[28] Attention is placed next on the low-q data of PF2/6/MCH-d_{14} and PF2/6$_{0.50}$-F8$_{0.50}$/MCH-d_{14}. Neither of the curves level off but show instead an upturn, which is consistent with the density fluctuations or aggregates of locally free chains with the size of ξ_s∼1700 Å (see Table 1). As the polymer concentration exceeds their overlapping concentration c^*, polymers are likely forming a loose network, even though the network contains 99% of solvent.

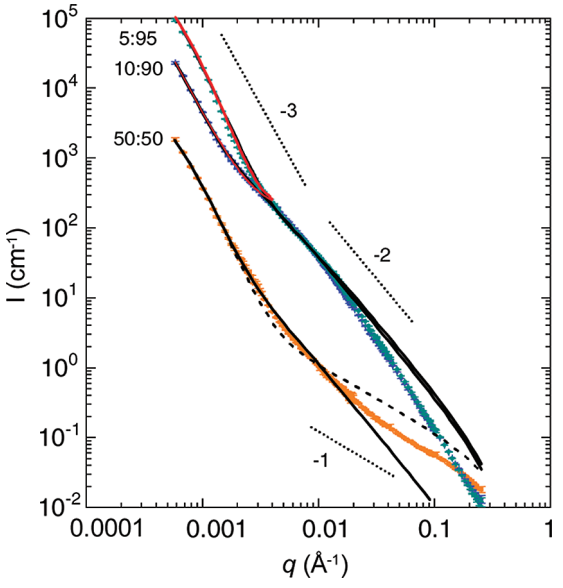

Figure 3. SANS patterns of PF2/6-F8 with the F2/6:F8 ratio 50:50 (orange up triangles), 10:90 (blue down triangles) and 5:95 (cyan solid circles) mixed with MCH-d_{14} (c = 10 mg/mL). Black lines are the fits to the two-component model. Black dashed line is a fit with an assumption of rodlike and black solid line lines with sheetlike scatterers (see Experimental Section for details). Red solid lines are fits to the eq 7. Black dotted lines show −1, −2, and −3 slopes for comparison.

These data with an upturn and subsequent q^{-1} scaling resemble those of poly(9,9-didecylfluorene) in MCH-d_{14}[14] and may be understood in terms of "segmental alignment" as introduced for PF8 in dense toluene solution by Rahman et al.[12] In this model, locally free chains are networked via nodes including mutually aligned polymer segments and this allows the modeling

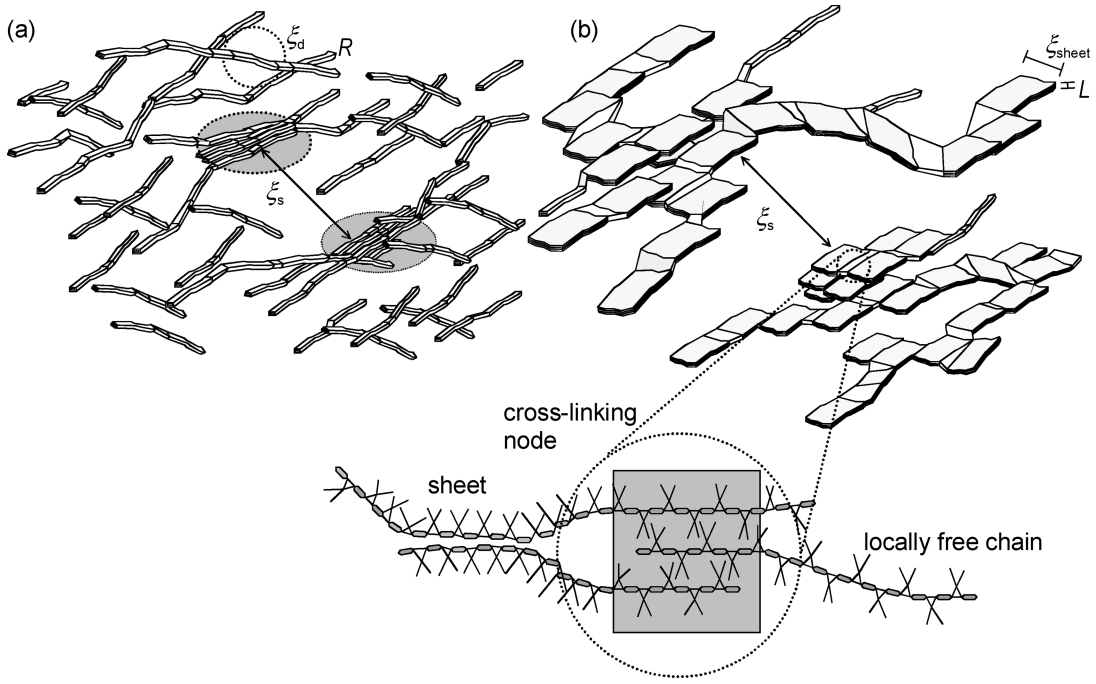

Figure 4. Illustrations of (a) overlapping rodlike polymers and (b) ribbonlike agglomerate of sheetlike aggregates. Also shown is the interpretation of parameters associated with the size of rodlike polymers (ξ_d, R), polymer sheets (ξ_{sheet}, L) and fluctuations in or within the networks (ξ_s).

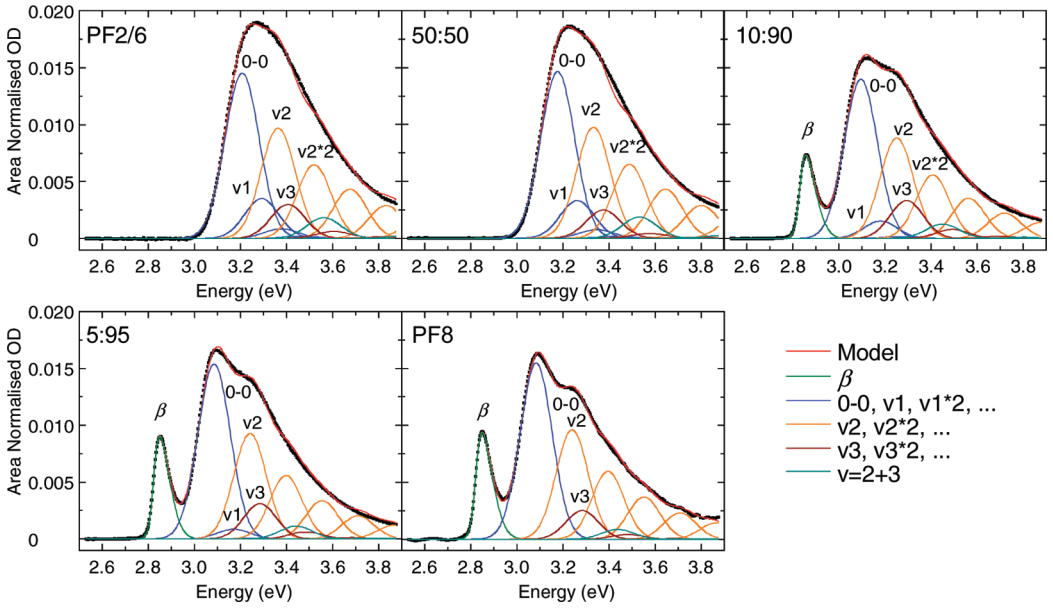

Figure 5. Area normalized optical density (OD) of PF2/6, PF2/6-F8 copolymers with the F2/6:F8 ratio 50:50, 10:90 and 5:95 and PF8 mixed with MCH (black symbols) and the overall model fitted to the data (red solid line). Also shown are fits to the spectral components 0−0 and $v1$ (blue), $v2$ (orange), $v3$ (brown), $v = (2 + 3)$ (cyan) and their multiplicities as well as the fit to the β peak (green). The notation vn^*m refers to the mth replica of the vibrational mode n.

of SANS data according to the eqs 4-6 (see Experimental Section). Yet it is clear that although the SANS curves of PF2/6/MCH-d_{14} and PF2/$6_{0.50}$-F$8_{0.50}$/MCH-d_{14} resemble each other and are qualitatively similar for $q > 0.02$ Å^{-1}, there are differences at lower q. The copolymer scatters more and has an upturn at lower scattering angle, the scattering characteristics thus being in between those of PF8/MCH-d_{14} and PF2/6/MCH-d_{14}.

Figure 3 shows the SANS data of PF2/6-F8 with the mixing ratios 50:50, 10:90 and 5:95 with the q-range of 0.00058−0.25 Å^{-1}. Also shown are the fits to the two-component model (eqs 4−6) with two different assumptions (rodlike polymers and sheetlike aggregates) for PF2/$6_{0.50}$-F$8_{0.50}$/MCH-d_{14} and with an assumption of sheetlike aggregates for other data. For comparison, the lowest q-range of the data of PF2/$6_{0.10}$-F$8_{0.90}$/MCH-d_{14} and

dx.doi.org/10.1021/ma201250h |*Macromolecules* 2011, 44, 6453–6460

PF2/$6_{0.05}$-F$8_{0.95}$/MCH-d_{14} are also fitted to equation 7 describing general fractal objects. Table 2 gives parameters estimated from these fits.

The data illustrate an effect of side chain branching, the decreased branching turning the scaling from $\sim q^{-1}$ to $\sim q^{-2}$ and the free rods into sheetlike structures when moving from PF2/$6_{0.50}$-F$8_{0.50}$/MCH-d_{14} to PF2/$6_{0.10}$- F$8_{0.90}$/MCH-d_{14}. All data show an upturn pointing to the larger length scale density fluctuations, which means that the rods and sheets are not isotropically distributed. Following the reasoning of ref 28, the rods are expected to form a loosely interleaved network while the sheets are assumed to form ribbonlike agglomerates with ordered cross-linking nodes. Figure 4 shows schematics of these arrangements.

Chen et al.[27] studied PF8/MCH and concluded that the system contains areas of "liquid crystal" phase with spatial fluctuations coexisting with an isotropic phase. The liquid crystals, or in our notation polymer sheets, are metastable and the system becomes macrophase separated with time. We suggest that the same holds for PF2/$6_{0.10}$-F$8_{0.90}$/MCH-d_{14} and PF2/$6_{0.05}$-F$8_{0.95}$/MCH-d_{14} such that they contain polymer sheets that are connected to ribbonlike agglomerates, these agglomerates coexisting with an isotropic phase. The tendency for macrophase separation over time increases with increasing side chain linearity.

When considering F$8_{0.50}$-PF2/$6_{0.50}$/MCH-d_{14} the data follow a qualitatively similar pattern as that of PF2/6/MCH-d_{14} but eqs 5 and 6 do not provide a good fit assuming solely rodlike or sheetlike scatterers (Figure 3). This implies that the polymer may show emerging local polymer aggregations albeit not yet fully developed polymer sheets. The dimensions associated with these models (ξ_d and ξ_s) are larger than those determined for PF2/6. Again, the nodes may correspond to "segmental alignment" as introduced in ref.[12]

When comparing PF2/$6_{0.10}$-F$8_{0.90}$/MCH-d_{14} and PF2/$6_{0.05}$-F$8_{0.95}$/MCH-d_{14}, the thickness (L) and lateral size of the sheetlike aggregates (ξ_{sheet}) are nearly independent of the side chain branching corresponding to the bilayers with the aspect ratio of >10 (Table 2). The dimensions of the larger length scale fluctuations (or agglomerates) (ξ_s) are also similar, and this length scale exceeds the length of individual polymers (<1000 Å). The scattering exponent α for <0.004 $Å^{-1}$ increases when going from PF2/$6_{0.10}$-F$8_{0.90}$/MCH-d_{14} to PF2/$6_{0.05}$-F$8_{0.95}$/MCH-d_{14}, which may indicate that a transition from mass fractal system to surface fractal system occurs, i.e., from the porous system to the system with compact core and fractal surface.

The low q part of the scattering curves of PF2/$6_{0.10}$-F$8_{0.90}$/MCH-d_{14} and PF2/$6_{0.05}$-F$8_{0.95}$/MCH-d_{14} can also be fitted to the structure factor of the general fractal object (eq 7) which we understand as an agglomerate of primary scatterers, phenomenologically corresponding to the outlined multicomponent model (eqs 4−6). Elsewhere the fractal interpretation has been successfully applied for diverse networks of π-conjugated polymers[38] and for example to describe large bilayers.[39] In this case the scattering exponent α, which represents the fractal dimension, is still larger for PF2/$6_{0.05}$-F$8_{0.95}$/MCH-d_{14}. Furthermore, the estimated dimensions of the primary scatterers and the whole objects are of the same order of magnitude as estimated from the two-component model. The fit parameters from both models also follow the same trend such that both are marginally larger for PF2/$6_{0.10}$-F$8_{0.90}$/MCH-d_{14}.

Figure 5 shows optical absorption data of the same samples. Also shown are modeled fits to the 0−0 peak, vibronic peaks $v1$, $v2$, and $v3$ with multiplicities as well as an asymmetric peak at

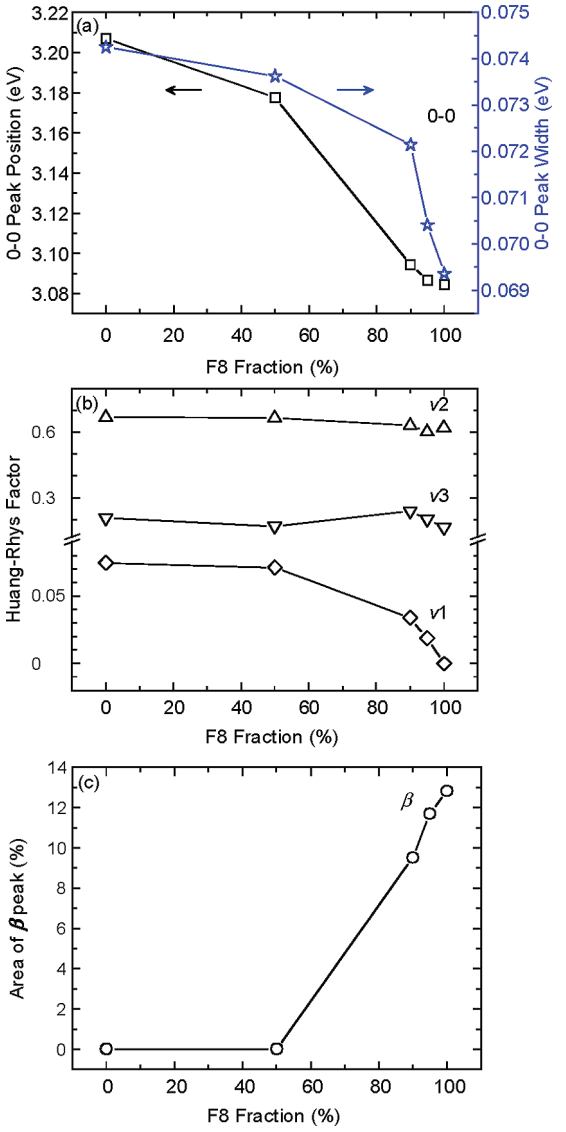

Figure 6. (a) Position (black open squares) and width (blue open stars) of 0−0 peak; (b) Huang−Rhys factors of vibrational components $v1$ (open diamonds), $v2$ (open up triangles), and $v3$ (open down triangles); and (c) the area of β peak (open circles) of PF2/6, PF2/6-F8 copolymers with the ratio 50:50, 10:90, and 5:95 and PF8 mixed with MCH. These values are estimated from the optical absorption data shown in Figure 5.

2.9 eV. The vibronic modes correspond to the energies 85 meV ($v1$), 156 meV ($v2$), and 199 meV ($v3$) and are identified from photoluminescence spectrum of PF8 and the spectra agree very well with the vibronic identification from Raman spectra.[40] The v_1 peak stems from the locally free chains without intermolecular contacts. The v_2 and v_3 peaks are attributed to the polymer aggregates with intermolecular contacts. The asymmetric peak originates (or even defines) the β phase. Main attention is placed on the strongest peaks seen in the range 2.8−3.4 eV. The location of the primary β phase vibronic replica approximately overlays the 0−0 of the aggregates and is not resolved, leading to a small underestimate of the fraction of β phase.

Figure 6 shows selected parameters estimated from the fits shown in Figure 5: The position and width of 0−0 peak, the Huang−Rhys factor for the selected spectral components and area of the

asymmetric β peak a function of side chain branching. The peak center of the main 0−0 band starts off near 3.08 eV for PF8 and smoothly increases to a maximum for pure PF2/6 [Figure 6a]. The Gaussian width parameter is narrowest for PF8 and increases smoothly in size to a maximum for PF2/6. There is a similar trend for the $v1$ peak Huang−Rhys factor indicating the presence of free chains which increases from nearly 0 to a maximum of 0.075 for PF2/6 [Figure 6b]. The β peak is seen for PF8/MCH and the copolymers with the fractions 10:90 and 5:95. This tendency is in accordance with the earlier results for PF8-DBT copolymers.[24]

The optical data indicate that the amount of free polymer chains is reduced as the F8 content increases, while the β phase follows polymer aggregation and visual gelation. This is in agreement with the idea that the β phase is located in the areas cross-linking polymer ribbons together, as proposed for linear side chain PFs as a function of side chain length.[28] In this model, the sheets are not entirely made of sheetlike β phase. The grain size of the β phase domains in PF8 mixed with MCH was found to be 120 Å as estimated from the corresponding X-ray diffraction peaks.[28]

Chen et al.[27] studied PF8/MCH by aging it tens of hours at room temperature. The authors described how the aggregation occurs through the spinodal decomposition mechanism, where the interconnected structure is arrested during the phase separation in a few hours, which leads to significant changes in light scattering data. This process can be accelerated by cooling (see for instance ref 25) in which case the aggregation begins in minutes, or by increasing polymer concentration. In the present work we have shown how this process can be controlled by varying the side chain branching. We expect that the copolymers follow the same gelation mechanism as PF8. Unlike Chen et al.,[27] we cannot follow similar time evaluation by neutron scattering but we note that the originally transparent PF2/$6_{0.10}$-F$8_{0.90}$/MCH-d_{14} and PF2/$6_{0.05}$-F$8_{0.95}$/MCH-d_{14} mixtures turn opaque yellowish gels without cooling in a few days. The PF2/6/MCH-d_{14} is still a clear liquid and PF2/$6_{0.50}$-F$8_{0.50}$/MCH-d_{14} solution shows a slight evidence of gelation but is still almost entirely clear liquid after a period of 8 weeks.

4. CONCLUSIONS

By using SANS and optical absorption we identify how the agglomeration of poly(9,9-dialkylfluorene)s depends on the alkyl side chain branching in MCH-d_{14} at room temperature. Polymers with 8 side chain carbons were used and the degree of branching was varied by copolymerizing branched side chain F2/6 units with linear side chain F8 units to form PF2/6-F8 copolymers. PF2/6/MCH-d_{14} appears as locally free chains that form a network of overlapping polymers. PF8/MCH-d_{14} contains sheetlike polymer aggregates that form a fractal network of ribbonlike agglomerates. PF2/6-F8/MCH-d_{14} shows similar network structure as PF2/6 for low F8 content but goes through a transition to agglomerate structure between 50% and 90% F8 addition. Optical absorption spectra are consistent with SANS results and indicate that the extent of locally free polymer decreases with increasing F8 content. In contrast, the β phase follows the existence of sheetlike structures, its fraction increasing sharply with increasing F8 content. It is plausible that the sheets include but are not entirely made of β phase. This work illustrates how well PF2/6-F8 suits the toolbox to study phase behavior of chemically similar but physically different polyfluorenes and the fine control one can achieve on complex polymer structures in this family of polyfluorene copolymers. Future work will include the synthesis of other PF2/6-F8 compositions and wide-angle X-ray scattering measurements. Furthermore, it will show to which extent these results can be generalized for other π-conjugated copolymers and polyfluorenes in particular.

AUTHOR INFORMATION

Corresponding Author
*E-mail: matti.knaapila@ife.no.

ACKNOWLEDGMENT

The SANS measurements were supported by the European Commission (Grant Agreement No. 226507-NMI3).

REFERENCES

(1) Scherf, U.; List, E. J. W. *Adv. Mater.* **2002**, *14*, 477–487.
(2) Cornil, J.; Gueli, I.; Dkhissi, A.; Sancho-Garcia, J. C.; Hennebicq, E.; Calbert, J. P.; Lemaur, V.; Beljonne, D.; Bredas, J. L. *J. Chem. Phys.* **2003**, *118*, 6615–6623.
(3) Inganäs, O.; Zhang, F. L.; Andersson, M. R. *Acc. Chem. Res.* **2009**, *42*, 1731–1739.
(4) Sirringhaus, H. *Adv. Mater.* **2005**, *17*, 2411–2425.
(5) Bliznyuk, V. N.; Carter, S. A.; Scott, J. C.; Klärner, G.; Miller, R. D.; Miller, D. C. *Macromolecules* **1999**, *32*, 361–369.
(6) Kamtekar, K. T.; Monkman, A. P.; Bryce, M. R. *Adv. Mater.* **2010**, *22*, 572–582.
(7) Knaapila, M.; Winokur, M. J. *Adv. Polym. Sci.* **2008**, *212*, 227–272.
(8) Justino, L. L. G.; Ramos, M. L.; Knaapila, M.; Marques, A. T.; Kudla, C. J.; Scherf, U.; Almásy, L.; Schweins, R.; Burrows, H. D.; Monkman, A. P. *Macromolecules* **2011**, *44*, 334–343. Lin, Z.-Q.; Shi, N.-E.; Li, Y.-B.; Qiu, D.; Zhang, L.; Lin, J.-Y.; Zhao, J.-F.; Wang, C.; Xie, L.-H.; Huang, W. *J. Phys. Chem. C* **2011**, *115*, 4418–4424.
(9) Fytas, G.; Nothofer, H. G.; Scherf, U.; Vlassopoulos, D.; Meier, G. *Macromolecules* **2002**, *35*, 481–488.
(10) Knaapila, M.; Stepanyan, R.; Lyons, B. P.; Torkkeli, M.; Monkman, A. P. *Adv. Funct. Mater.* **2006**, *16*, 599–609.
(11) Grell, M.; Bradley, D. D. C.; Long, X.; Chamberlain, T.; Inbasekaran, M.; Woo, E. P.; Soliman, M. *Acta Polym.* **1998**, *49*, 439–444.
(12) Rahman, M. H.; Chen, C.-Y.; Liao, S.-C.; Chen, H.-L.; Tsao, C.-S.; Chen, J.-H.; Liao, J.-L.; Ivanov, V. A.; Chen, S.-A. *Macromolecules* **2007**, *40*, 6572–6578.
(13) Knaapila, M.; Lyons, B. P.; Hase, T. P. A.; Pearson, C.; Petty, M. C.; Bouchenoire, L.; Thompson, P.; Serimaa, R.; Torkkeli, M.; Monkman, A. P. *Adv. Funct. Mater.* **2005**, *15*, 1517–1522. Knaapila, M.; Stepanyan, R.; Torkkeli, M.; Lyons, B. P.; Ikonen, T. P.; Almásy, L.; Foreman, J. P.; Serimaa, R.; Güntner, R.; Scherf, U.; Monkman, A. P. *Phys. Rev. E* **2005**, *71*, 041802.
(14) Knaapila, M.; Stepanyan, R.; Torkkeli, M.; Garamus, V. M.; Galbrecht, F.; Nehls, B. S.; Preis, E.; Scherf, U.; Monkman, A. P. *Phys. Rev. E* **2008**, *77*, 051803.
(15) Dias, F. B.; Knaapila, M.; Monkman, A. P.; Burrows, H. D. *Macromolecules* **2006**, *39*, 1598–1606.
(16) Rothe, C.; Galbrecht, F.; Scherf, U.; Monkman, A. *Adv. Mater.* **2006**, *18*, 2137–2140.
(17) Yap, B. K.; Xia, R.-D.; Campoy-Quiles, M.; Stavrinou, P. N.; Bradley, D. D. C. *Nat. Mater.* **2008**, *7*, 376–380.
(18) Shi, H.-F.; Nakai, Y.; Liu, S.-J.; Zhao, Q.; An, Z.-F.; Tsuboi, T.; Huang, W. *J. Phys. Chem. C* **2011**, *115*, 11749–11757.
(19) Charas, A.; Morgado, J.; Alcácer, L.; Brogueira, P.; Cacialli, F. *Synth. Met.* **2004**, *147*, 275–279.
(20) Traiphol, R.; Charoenthai, N.; Manorat, P.; Pattanatornchai, T.; Srikhirin, T.; Kerdcharoen, T.; Osotchan, T. *Synth. Met.* **2009**, *159*, 1224–1233.
(21) Cheun, H.; Galbrecht, F.; Nehls, B.; Scherf, U.; Winokur, M. J. *J. Mater. Sci.: Mater. Electron.* **2009**, *20*, 498–504. Cheun, H.; Galbrecht,

F.; Nehls, B. S.; Scherf, U.; Winokur, M. J. *J. Lumin.* **2007**, *122*−*123*, 212–217.
(22) Knaapila, M.; Torkkeli, M.; Monkman, A. P. *Macromolecules* **2007**, *40*, 3610–3614.
(23) Monkman, A.; Rothe, C.; King, S.; Dias, F. *Adv. Polym. Sci.* **2008**, *212*, 187–225.
(24) Bright, D. W.; Moss, K. C.; Kamtekar, K. T.; Bryce, M. R.; Monkman, A. P. *Macrom. Rapid Comm.* **2011**, *32*, 983–987.
(25) Knaapila, M.; Garamus, V. M.; Dias, F. B.; Almásy, L.; Galbrecht, F.; Charas, A.; Morgado, J.; Burrows, H. D.; Scherf, U.; Monkman, A. P. *Macromolecules* **2006**, *39*, 6505–6512.
(26) Dias, F. B.; Morgado, J.; Macanita, A. L.; da Costa, F. P.; Burrows, H. D.; Monkman, A. P. *Macromolecules* **2006**, *39*, 5854–5864.
(27) Chen, C.-Y.; Chang, C.-S.; Huang, S.-W.; Chen, J.-H.; Chen, H.-L.; Su, C.-I.; Chen, S.-A. *Macromolecules* **2010**, *43*, 4346–4354.
(28) Knaapila, M.; Bright, D. W.; Stepanyan, R.; Torkkeli, M.; Almásy, L.; Schweins, R.; Vainio, U.; Preis, E.; Galbrecht, F.; Scherf, U.; Monkman, A. P. *Phys. Rev. E* **2011**, *83*, 051803.
(29) Ying, Q.; Chu, B. *Macromolecules* **1987**, *20*, 362–366.
(30) Grell, M.; Bradley, D. D. C.; Ungar, G.; Hill, J.; Whitehead, K. S. *Macromolecules* **1999**, *32*, 5810–5817.
(31) Chen, J.-H.; Chang, C.-S.; Chang, Y.-X.; Chen, C.-Y.; Chen, H.-L.; Chen, S.-A. *Macromolecules* **2009**, *42*, 1306–1314.
(32) Stuhrmann, H. B.; Burkhardt, N.; Dietrich, G.; Jünemann, R.; Meerwinck, W.; Schmitt, M.; Wadzack, J.; Willumeit, R.; Zhao, J.; Nierhaus, K. H. *Nucl. Instrum. Methods A.* **1995**, *356*, 124–132.
(33) Wignall, G. D.; Bates, F. S. *J. Appl. Crystallogr.* **1987**, *20*, 28–40.
(34) Schmidt, P. W. Some Fundamental Concepts and Techniques Useful in Small-Angle Scattering Studies of Disordered Solids. In *Modern Aspects of Small-Angle Scattering*; Brumberger, H., Ed.; Kluwer Academic Publishers: Dordrecht, The Netherlands, 1995; pp 1−56.
(35) Svergun, D. I. *J. Appl. Crystallogr.* **1992**, *25*, 495–503.
(36) Shibayama, M. *Macrom. Chem. Phys.* **1998**, *199*, 1–30.
(37) Teixeira, J. Experimental Methods for Studying Fractal Aggregates. In *On Growth and Form*; Stanley, H. E., Ostrovsky, N., Eds.; Nijhoff: Dordrecht, The Netherlands, 1986; pp 145−162.
(38) Li, Y.-C.; Chen, K.-B.; Chen, H.-L.; Hsu, C.-S.; Tsao, C.-S.; Chen, J.-H.; Chen, S.-A. *Langmuir* **2006**, *22*, 11009–11015. Li, Y.-C.; Chen, C.-Y.; Chang, Y.-X.; Chuang, P.-Y.; Chen, J.-H.; Chen, H.-L.; Hsu, C.-S.; Ivanov, V. A.; Khalatur, P. G.; Chen, S.-A. *Langmuir* **2009**, *25*, 4668–4677.
(39) Vogtt, K.; Jeworrek, C.; Garamus, V. M.; Winter, R. *J. Phys. Chem. B* **2010**, *114*, 5643–5648.
(40) Ariu, M.; Lidzey, D. G.; Bradley, D. D. C. *Synth. Met.* **2000**, *111*−*112*, 607–610.